Research Article | Vol. 30, No. 8 / 11 Apr 2022 / Optics Express 12982
Optics EXPRESS

Performance optimization of a metasurface incorporating non-volatile phase change material

NATSIMA SAKDA,[1,2,*] SOUVIK GHOSH,[3] RATCHAPAK CHITAREE,[1] AND B. M. AZIZUR RAHMAN[2]

[1]Department of Physics, Faculty of Science, Mahidol University, Bangkok 10400, Thailand
[2]School of Mathematics, Computer Science and Engineering, City, University of London, London EC1 V 0HB, UK
[3]Department of Electronic and Electrical Engineering, University College London, London WE1C 6BT, UK
[*]natsima.sad@student.mahidol.ac.th; natsima.sakda@city.ac.uk

Abstract: Optical metasurface is a combination of manufactured periodic patterns of many artificial nanostructured unit cells, which can provide unique and attractive optical and electrical properties. Additionally, the function of the metasurface can be altered by adjusting the metasurface's size and configuration to satisfy a particular required property. However, once it is fabricated, such specific property is fixed and cannot be changed. Here, phase change material (PCM) can play an important role due to its two distinct states during the phase transition, referred to as amorphous and crystalline states, which exhibit significantly different refractive indices, particularly in the infrared wavelength. Therefore, a combination of metasurface with a phase change material may be attractive for achieving agile and tunable functions. In this paper, we numerically investigate an array of silicon cylinders with a thin PCM layer at their centers. The GST and GSST are the most well-known PCMs and were chosen for this study due to their non-volatile properties. This structure produces two resonant modes, magnetic dipole and electric dipole, at two different resonating wavelengths. We have numerically simulated the effect of cylinder's height and diameter on the reflecting profile, including the effect of thickness of the phase change material. Additionally, it is shown here that a superior performance can be achieved towards reduced insertion loss, enhanced extinction ratio, and increased figure of merit when a GST layer is replaced by a GSST layer.

1. Introduction

Metasurfaces are artificially engineered material which have been widely investigated due to their exotic optical properties. These properties can be easily customized and modified by two main factors: (i) considering the arrangement of unit cells which can be assumed as the subwavelength building block of a metasurface, and (ii) the shape and design of the periodic pattern of the unit cell [1–4]. The unique properties of metasurface can achieve several superior performances such as perfect absorption [5,6], extraordinary optical transmission [7] and frequency selective surface [8,9]. Metasurface can be used in various applications, for example as an absorber [6,10,11], perfect lens [12], polarizer [13,14], imaging and information process [15–17], and biological and chemical sensings [18]. However, once the designed device with its attractive optical characteristics has been fabricated, its property remains unchanged through its usage time. Such fixed properties can limit the wider implementation of these devices. Therefore, the tunable metasurface is now a new area of research and several tunable metasurfaces [19–22] have been studied, either electrically or geometrical parameters scaling tuning.

Phase Change Materials (PMCs) are the materials that have two very distinct states, called crystalline and amorphous states. These two-phase transitions have drawn considerable attention

#453612 https://doi.org/10.1364/OE.453612
Journal © 2022 Received 11 Jan 2022; revised 24 Mar 2022; accepted 24 Mar 2022; published 4 Apr 2022

Optics EXPRESS

due to their unique optical properties and their fast, agile manipulation of transition process which can be easily controlled by using a pulse of short duration, in the order of sub-nanosecond [23,24] for a complete phase change. The transition between crystalline and amorphous states can be externally excited by using optical [25,26] or electrical pulse [27–29]. Recently, the phase change material based on chalcogenide alloys, Germanium-Antimony-Tellurium (GST) has become more attractive because of its non-volatile performance [30], when its stable state can be maintained without any continuous energy consumption. This opens up a number of new possibilities, such as phase-change neurons [31,32], phase-change photonic memory [33,34], phase-change metamaterials and metasurface [35–39]. The majority research of using PCM is mostly focused on GST, however another new type of PCM, called GSST has recently been reported by Zhang *et al.* [40] which particularly shows low loss at the telecom wavelength. This new PCM material can be created by partially substituting the tellurium in the GST with selenium atoms, which has a lower optical loss in the crystalline and amorphous states [41,42]. Therefore, integration of GSST in the metamaterial could lead to an enhanced performance of its switchable properties.

In this paper, the effects of the geometrical parameters including height, diameter of the cylinder structure and thickness for GST and GSST have been thoroughly studied. In addition, the performance of GST and GSST in terms of the reflectance contrast, the Insertion Loss (IL), the Extinction Ratio (ER) and the Figure of Merit (FOM) are also compared.

2. Designed structure

The schematic design of the unit cell is depicted in Fig. 1(a). The unit cell considered here is a silicon cylinder with its height, H and diameter, D. A thin phase change material (PCM) of thickness, T, made from either GST or GSST is inserted in the middle of the cylinder. The periodically arranged array of unit cells are placed on top layer of a silicon dioxide buffer layer as shown in Fig. 1(b). Moreover, the incident field that have been used for the numerical simulations is shown above the periodic pattern, compose of an electric field in the x-direction ($\mathbf{E_x}$) along with a magnetic field in the y-direction ($\mathbf{H_y}$), and both are perpendicular to the propagation direction (z) of the wave into the structure.

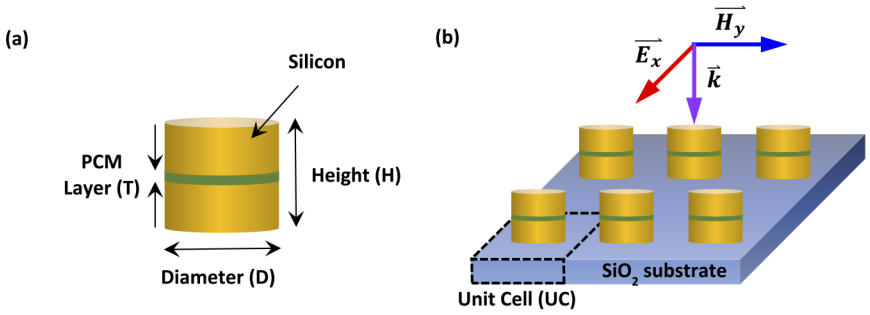

Fig. 1. (a) Geometrical structure of the unit cell. The silicon cylinder with height (H) and diameter (D) and a PCM layer of a thickness (T) at the center. (b) The unit cell is placed on a silicon dioxide buffer layer.

Here, Fig. 2(a) shows the refractive indices of silicon [43] and silica (SO_2) [44] using solid green and orange lines, respectively. On the other hand, the refractive indices of GST [45] and GSST [46] are shown in Figs. 2(b) and 2(c), respectively. The real part of their refractive indices at the amorphous and crystalline states, are shown by solid red and blue lines, whereas, their loss coefficients, k are shown by dashed red and blue lines, respectively. It can be observed that the loss coefficients of the GSST in both the states are much smaller than that of the GST and thus it

Optics EXPRESS

is expected to lead to a higher performance when GST is replaced by GSST, as shown in our study.

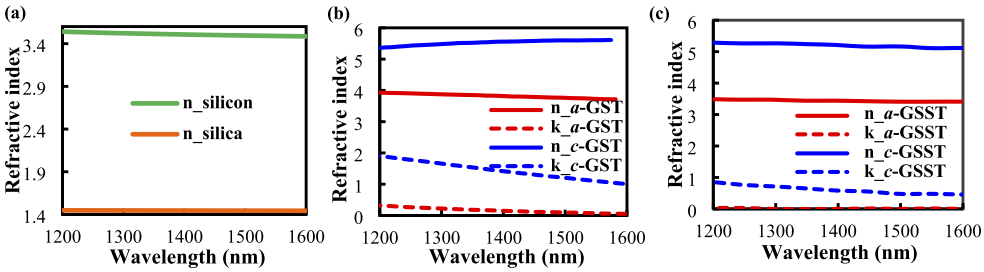

Fig. 2. (a) Dielectric constant of silicon and silica in blue and orange lines, respectively. The Refractive indices of both GST (b) and GSST (c) which are used in this study. The red and blue lines represent material in the amorphous and the crystalline states, respectively.

3. Numerical and optimization process

Numerical analyses of this work start by using the Finite Element Method (FEM) and examining the reflectance profile and the behavior of resonant wavelengths of this proposed structure.

3.1. Reflectance profile

In this study, we aim to maximize the reflectance contrast between the amorphous and crystalline states of phase change material. At the start, for bench marking, we considered the reported work of [45] at the telecom wavelength of 1550 nm. Here, the silicon cylinder structure with its diameter of 660 nm, height of 198.4 nm, the GST thickness of 15 nm and periodicity of 850 nm was studied for the reflectance profile of the unit cell. To obtain the agreement pattern and resonant wavelength at 1550 nm, the diameter and height need to slightly modify from 666 nm to 660 nm and 195 nm to 198.4 nm, respectively.

Two sets of the reflectance spectra are shown in Fig. 3. The reflectance values from our work for crystalline and amorphous states are shown by red solid and dashed lines, respectively. Additionally, the reflectance values reported by De Galarreta *et al.* for the crystalline and amorphous states are shown by blue solid and dashed lines, respectively. The numerical results indicate that the designed unit cell provide two resonant modes; one around 1300 - 1350 nm and another exactly at 1550 nm. The first mode from the unit cell structure has a high value of reflectivity (0.93) at 1333 nm in the amorphous state (*a*-state). While GST is changed to the crystalline state (*c*-state), the first resonant mode is slightly shifted from 1333 nm to 1331 nm and the reflectance is also dropped slightly to 0.70. For the second resonant mode, the reflectivity of *a*-state is 0.81 at 1550 nm. However, when the phase of GST is changed to the *c*-state, the second resonant mode is almost vanished due to a large change in refractive indices (reflectance value of only 0.14). Our result is in good agreement with the reported one [45]. The resonance at the higher wavelength is known as Electric Dipole (ED) and at the lower wavelength is known as Magnetic Dipole (MD). Later on, we will present their dominant field profiles which will help to understand their behaviors. The unit cell structure has two modes of resonant wavelengths, in which the first mode remains almost unchanged during the phase transition while the second mode is changed significantly in the crystalline state. The reflectance difference between amorphous and crystalline state is commonly defined as reflectance contrast (RC) which is the difference in

Optics EXPRESS

reflectivity between these two phases transitions;

$$RC = R_a - R_c \tag{1}$$

where R_a and R_c are the reflectances of the unit cell structure in the amorphous and crystalline states, respectively. From the Fig. 3, it is found that the reflectance contrast of the second mode (at 1550 nm) between the two states is 0.67. The reflectance contrast can be used to evaluate the performance of a tunable reflector as functions of geometrical parameters. In summary, the unit cell structure has shown two modes with two different resonant wavelengths. The first mode does not change much during the phase transition, however, the second mode is changed significantly in the crystalline state.

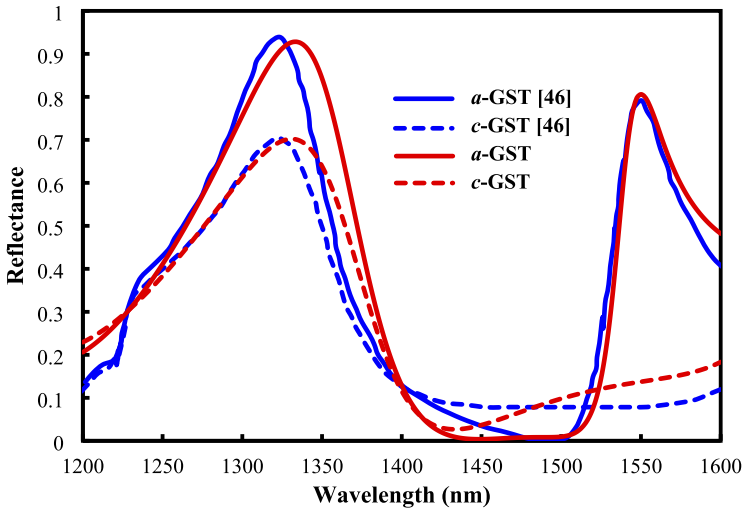

Fig. 3. The comparison of reflectance profiles between the reference paper [45] and the numerical calculation from this work. The solid lines are *a*-state and the dash lines are *c*-state.

To understand the behavior of these two sets of dipoles, the mode field distribution at these two peaks are shown in Fig. 4. For the first mode, the electric and magnetic field contours are shown in Figs. 4(a) and 4(b), respectively. To have a better view of their behaviors, fields close to the cylinder are only shown. For this mode, in *a*-GST state, it can be seen that the magnetic field has maximum values at the center of the Si disk (along the PCM layer) like a fundamental H mode (Fig. 4(b)). On the other hand, **E** field value is minimum at the center of the cylinder for this resonance with a higher order spatial variation (Fig. 4(a)). Therefore, this resonance peak is known as the Magnetic Dipole (MD). So, for the transition of the PCM to *c*-GST, although its refractive index is changed significantly in the PCM layer, the modal properties of MD is only slightly changed (but not shown here) resulting only a small change of the MD resonance. However, for the second peak, in *a*-GST state, the maximum **E**-field is at the center of disk with its spatial distribution like a fundamental E mode (Fig. 4(c)). Therefore, this resonance peak is known as the Electric Dipole (ED). The modal properties of the ED peak change significantly for the *c*-GST state to accommodate the large index change. Due to the large increase in its metallic behavior, the electric field at the center change significantly and the resulting reflectance is reduced considerably.

Optics EXPRESS

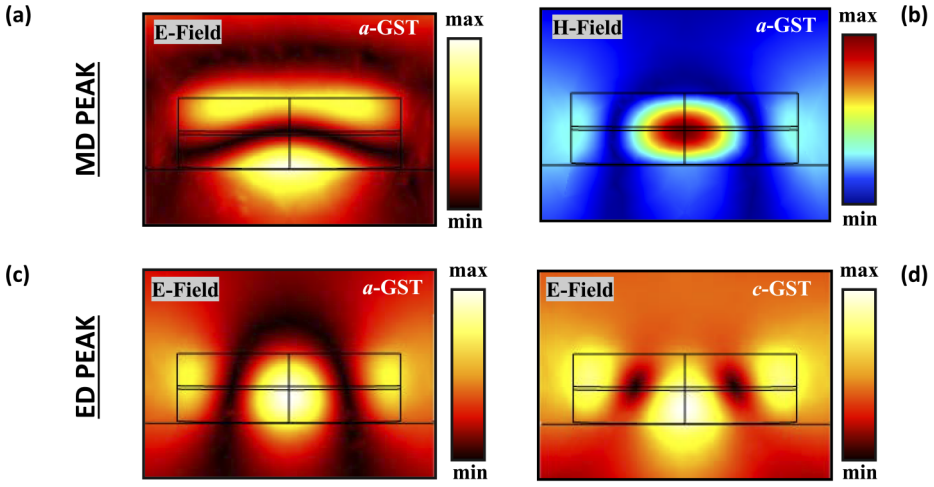

Fig. 4. The electric and magnetic field distributions: (above) for the magnetic dipole, (below) for the electric dipole. The rectangular shape drawn by solid lines represent a unit cell structure.

3.2. *Geometrical parameter effect*

To study the effects of height and diameter of the unit cell on the resonating wavelengths for magnetic diploe (λ_{MD}) and electric diploe (λ_{ED}), respectively, numerical simulations have been carried out. As the phase transition of PCM significantly influences the reflectance of electric dipole, we selectively focus on the resonant wavelength of this electric dipole, λ_{ED}.

Variations of the λ_{ED} with the diameter for 4 different heights are shown in Fig. 5. It can be seen that as diameter is increased, λ_{ED} values also increased linearly. In addition, it can be noted that for higher cylinder height, H, the resonant frequency is also higher. This is expected as for all electromagnetic device its performances can be scaled by dimensions normalized to its wavelength. Our desired λ_{ED} = 1550 nm is shown by a horizontal dash line.

From this, for a given cylinder height, its diameter can be adjusted to have λ_{ED} exactly at 1550 nm. Here, the dimensions are selected such that, in all cases, the resonant wavelength λ_{ED} = 1550 nm can be achieved. This is clearly confirmed by three geometrical conditions, which are H = 215 nm with D = 646.8 nm, H = 195 nm with D = 663 nm, and H = 175 nm with D = 684.6 nm as seen from Fig. 6. The optimization process executed for each height of cylinder with its matching diameter, so these structures can provide the electric dipole at 1550 nm.

Variations of the reflectance for H = 215 nm, 195 nm, and 175 nm are shown in Fig. 6 by blue, red, and green lines, respectively. Reflectance for *a*-state and *c*-state are shown by solid and dashed lines, respectively. The value reflectances at λ_{ED} are calculated as 0.79, 0.81 and 0.81 for H = 215, 195 and 175 nm, respectively, in the *a*-state. However, in the *c*-state, the reflectance at λ_{ED} gradually decreases to 0.24, 0.10 and 0.05 when H = 215, 195 and 175 nm, respectively. The reflectance contrast of between the states is 0.74, 0.71, and 0.57, for H = 215, 195, and 175 nm, respectively. The decreasing reflectance in *c*-state at λ_{ED} is due to the shift of λ_{MD} to the higher wavelengths. The reflectance at *a*-state for the magnetic dipole were 0.94, 0.93, and 0.91 for H = 215, 195, and 175 nm and shown by solid blue, red, and green lines, respectively. However, in the *c*-state (shown by dashed lines), the reflectance at λ_{MD} slightly decreases to 0.72, 0.70, and 0.68. for H = 215, 195, and 175 nm, respectively.

Next, variation of the required diameter D for a given height H, to achieve λ_{ED} = 1550 nm is shown by a red curve in Fig. 7. It can be noted that, to achieve the resonant wavelength of the electric dipole at 1550 nm, with the increasing height, its diameter needs to be decreased.

Optics EXPRESS

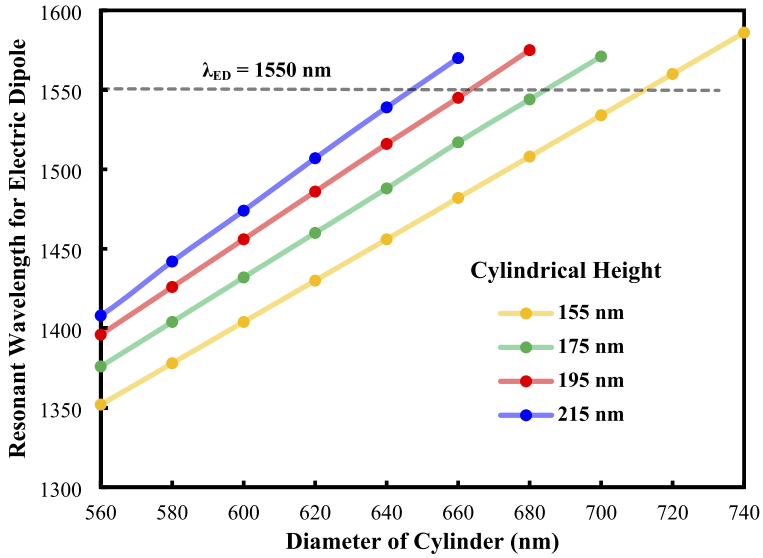

Fig. 5. The relation between λ_{ED} when varying the diameter of cylinder at the different cylindrical height.

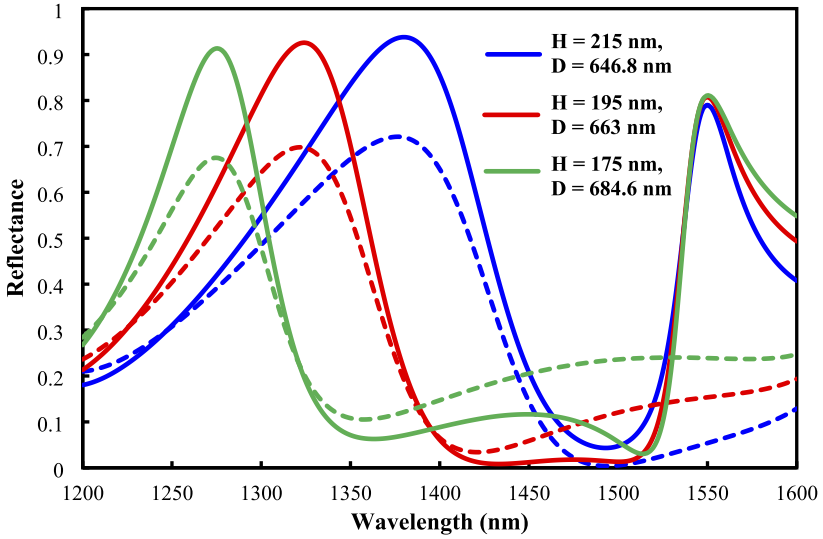

Fig. 6. The optimized reflectance for heights and diameters that give the resonant wavelength of the electric dipole at 1550 nm. Blue, red and green lines represent reflectance from different pairs of H&D. Solid lines are *a*-state and dash lines are *c*-state.

Optics EXPRESS

However, if height of the cylinder increases, the resonant wavelength of magnetic dipole is significantly affected as shown by a blue line. The magnetic dipole wavelength is shifted to longer wavelengths directly proportional to the cylindrical height.

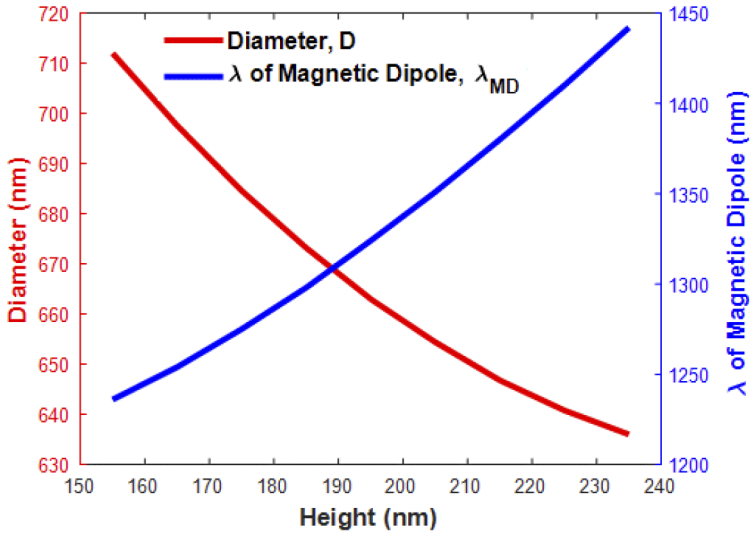

Fig. 7. (Red line) The relation between height and diameter. (Blue line) The relation between height and magnetic dipole resonant wavelength when $\lambda_{ED} = 1550$ nm. (Considered when GST takes place in amorphous state)

Apart from considering the reflectivity at the ED resonant wavelength for both amorphous and crystalline states, there are two more important parameters which can be used to evaluate the performance of the proposed unit cell reflector, and these can be defined as:

$$Insertion\ Loss(IL) = -10\log_{10} R_{a\ at\ \lambda_{ED}} \tag{2}$$

and

$$Extinction\ Ratio\ (ER) = 10\log_{10} \frac{R_{a\ at\ \lambda_{ED}}}{R_{c\ at\ \lambda_{ED}}} \tag{3}$$

Where $R_{a\ at\ \lambda_{ED}}$ and $R_{c\ at\ \lambda_{ED}}$ are the reflectance of the electric dipole at amorphous and crystalline states of GST, respectively.

Variations of Insertion Loss (IL) and Extinction Ratio (ER) with the cylindrical height (H) are shown by red and blue lines, respectively in Fig. 8. The main objectives of designing a switchable unit cell reflector could be to minimize the Insertion Loss and at the same time, to maximize the Extinction Ratio. As can be seen from Fig. 8, that around 185 nm height of the cylinder, the IL is minimum while the value of ER is rather quite low. The ER increases as cylinder height, H is increased and reaches a maximum value of 28 dB around Height = 230 nm. However, the IL is also dramatically increased. From this figure, a suitable design can be chosen to provide the optimum performances of the proposed phase change material, as needed for a particular application.

3.3. Effect of the phase change material thickness

In the previous section, the effect of height and diameter of Fig. 9. The optimized reflectance profile for GST layer to get the electric dipole at 1550 nm. Blue, red and green lines represent different T&H conditions. Solid lines are for *a*-state and dash lines are for *c*-state. the cylinder

Optics EXPRESS

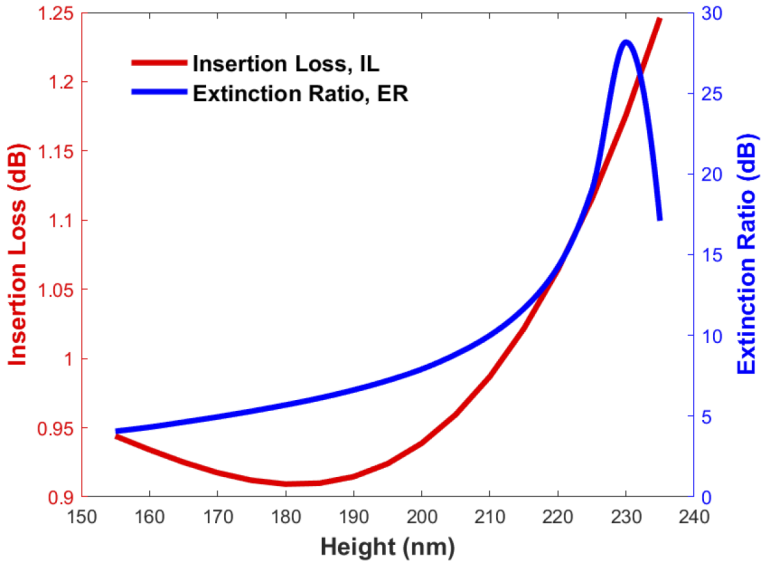

Fig. 8. The insertion loss (considered from the amorphous state of GST) and the extinction ratio at the different height (which related to each diameter in Fig. 7) of cylinder of the electric dipole mode at 1550 nm.

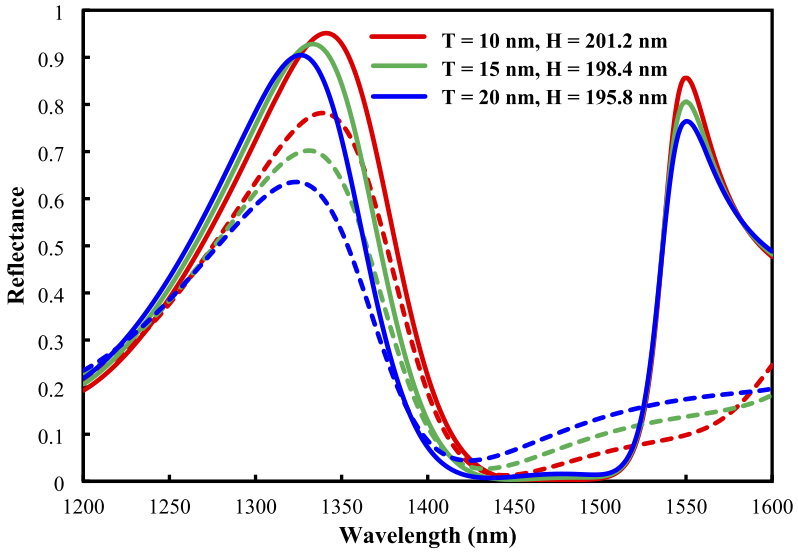

Fig. 9. The optimized reflectance profile for GST layer to get the electric dipole at 1550 nm. Blue, red and green lines represent different T&H conditions. Solid lines are for *a*-state and dash lines are for *c*-state.

Optics EXPRESS

were investigated on the reflectance profile, with a 15 nm fixed thickness of the phase change material layer. In this section, the effect of the PCM thickness is investigated.

Three different thicknesses of the phase change material are considered, 10 nm, 15 nm and 20 nm, and the diameter of silicon cylinder is fixed at 660 nm. This is obvious that the thickness change of the GST layer also results in the slight shifts of resonating wavelength for both magnetic and electric dipoles and so the overall height is slightly adjusted to obtain the electric dipole at the 1550 nm. The corresponding H values are 201.2, 198.4, and 195.8 nm when the T was chosen for 10, 15, and 20 nm, respectively. Variations of reflectance with the operating wavelength for three different GST thicknesses are shown in Fig. 9. The solid lines represent the reflectance when GST is in amorphous state while the dash lines show when the GST is in crystalline state.

From Fig. 9, we can observe that the electric dipole, λ_{ED} at 1550 nm, as designed. But the reflectance level is different for each GST thickness and these values are 0.86, 0.81, and 0.76 for 10 nm, 15 nm, and 20 nm of GST thicknesses, respectively, in the amorphous state. It can be noted that the loss is lower for smaller thickness of GST. As the GST phase is changed to the crystalline state, the electric dipole mode is nearly vanished as expected. Moreover, we can observe that the magnetic dipole that located at the shorter wavelength is shifted to the longer wavelength when the thickness of GST is thinner. The reflectivity at 1550 nm in *c*-state are 0.1, 0.14, and 0.17 for the thickness of 10 nm, 15 nm, and 20 nm, respectively. It can be observed that a lower thickness of GST provides a better performance.

Variations of the Insertion Loss (IL) and Extinction Ratio (ER) with the GST thickness are shown in Fig. 10, by red and blue curves, respectively. In this case, D was fixed at 660 nm, however, H was adjusted to achieve the λ_{ED} to be exactly at 1550 nm. It can be observed that as the GST thickness reduces, the insertion loss also reduces, and the extinction ratio increases. This suggests that the GST layer thickness should be reduced to obtain a better performance of the proposed structure. However, it may be difficult to fabricate a very thin PCM layer and the effect of a small change in the thickness would result in a large change in the unit cell performance. So, for further investigations, a moderate value of T = 10 nm is chosen.

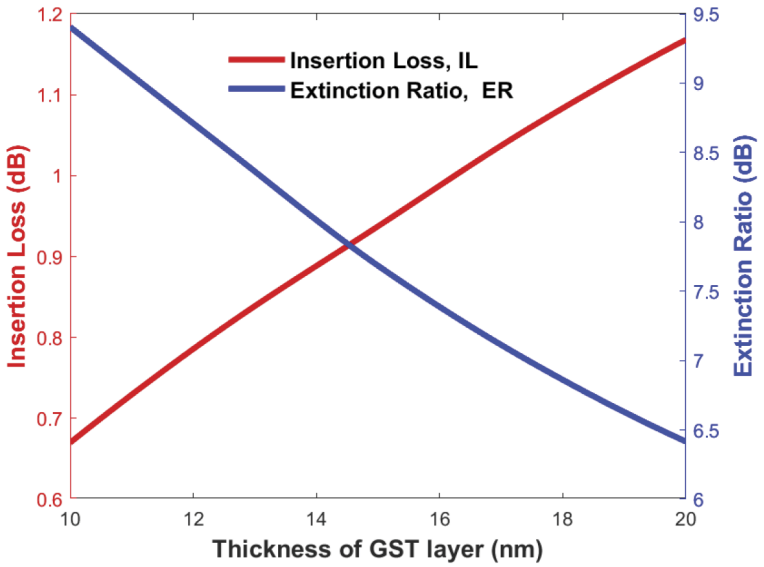

Fig. 10. The insertion loss (considered from the amorphous state of GST) and the extinction ratio at the different GST Thickness of the electric dipole mode at 1550 nm.

Optics EXPRESS

Recently, is has been reported that [41,42] the loss of GSST is significantly lower compared to the more established GST at the telecom wavelengths. Next, the effect of the phase change material by replacing the GST with GSST is studied. However, as expected, by replacing the GST by GSST, the reflectance peaks for both magnetic and electric dipoles will shift to a shorter wavelength. Therefore, the optimization process was performed in order to adjust the electric dipole to be located exactly at the 1550 nm. The thickness of replacing GSST was selected as 10 nm. The optimized geometrical parameters that generated the required reflectance spectrum are H = 208 nm and D = 660 nm.

Figure 11 shows the reflectance profile of the proposed structure with red solid lines for *a*-GSST and dashed lines for *c*-GSST. The performance of this structure shows a very high reflectivity in amorphous GSST for both magnetic and electric dipoles at 1360 nm and 1550 nm with reflectivity of 0.996 and 0.96, respectively, which is due to low loss coefficient of GSST. When the phase transition of GSST is changed to crystalline, the λ_{MD} still has a reasonably high reflectivity of 0.9 at 1362 nm. However, the reflectivity at the λ_{ED} =1550 nm in *c*-state is very low with a value of 0.02. This clearly provides a significant reflectance contrast between *a*-GSST and *c*-GSST states (RC = 0.94). Figure 11 also shows the comparison between the result in this study (illustrated in red solid and dashed lines) to the one reported in [45] shown by blue solid and dash lines. For the magnetic dipole, even though, their resonant MD modes do not match, our proposed structure offers a significantly higher reflectivity for both the phase transitions. Moreover, for the electric dipole, not only the reflectivity at 1550 nm is higher in *a*-state but also lower in the crystalline state. Subsequently, this leads to a greater reflectance contrast. The benchmark performance for the proposed unit cell are calculated at the insertion loss of only 0.18 dB and the extinction ratio of 16.8 dB.

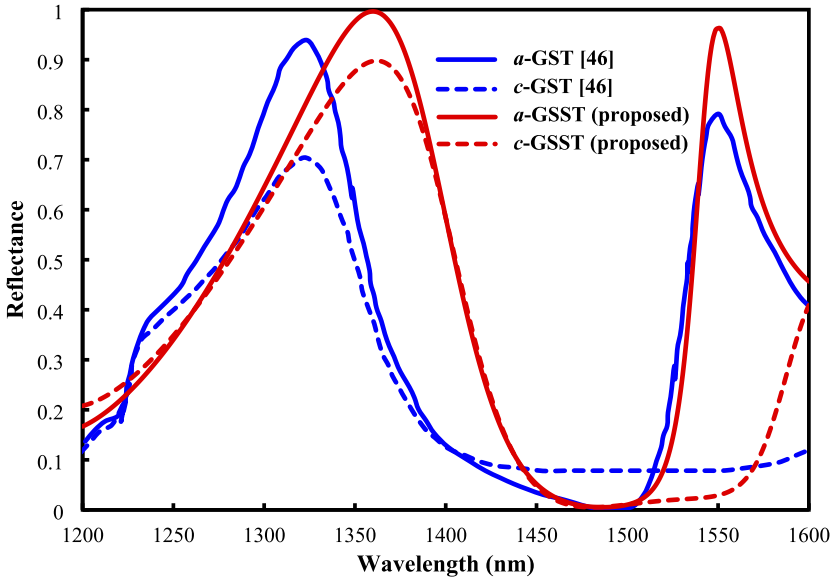

Fig. 11. The reflectance profile comparing between the proposed GSST included unit cell and the reflectance profile from the reference work [45]. Solid lines are for *a*-state and dashed lines are for c-state.

Figure of Merit (FOM) is one key parameter that can be used to describe the PCM performance. The FOM is defined as

$$FOM = \frac{ER}{IL} \tag{4}$$

Optics EXPRESS

Where the ER and IL are the extinction ratio and the insertion loss as already defined in Eqs. (2) and (3). The summary of the proposed PCM performance based on all mentioned structures in this work in comparison to the reference research [45] is shown in Table 1.

Table 1. The comparison performance of the unit cell structures that have been designed in this work

	H (nm)	D (nm)	T (nm)	IL (dB)	ER (dB)	FOM
[45]	195	666	15(GST)	1.02	10.5	10.3
1	215	646.8	15(GST)	1.02	12.0	11.2
2	201.2	660	10(GST)	0.66	9.3	14.1
3	208	660	10(GSST)	0.18	16.8	93.3

The first condition (1) is when the height of the cylinder was significantly reduced and the radius was adjusted to achieve the same λ_{ED} = 1550 nm, and result was shown in Fig. 8. The second condition (2) is when the thickness of GST was decreased to 10 nm and also the height and diameter were optimized to achieve λ_{ED} = 1550 nm and this was shown in Fig. 9. Finally, the third condition (3), when the GST layer is replaced by the GSST in which the PCM thickness equal to 10 nm was shown in Fig. 11. From the summary table, we can observe that the most promising unit cell structure is from the third condition. This is because IL is minimized and ER is maximized at the same time and subsequently FOM becomes the maximized.

4. Conclusion

In this work, we have focused on the numerical study of a controllable reflector incorporating silicon cylinder with PCM at the center. The main characteristic of reflectance spectrum is the two resonant wavelengths when the phase change material (which is placed at the middle of cylinder) is in the amorphous state. These two modes are identified as the magnetic and electric dipoles from the field distribution at these resonances. When the PCM is changed the phase into crystalline state, the magnetic dipole remains nearly the same. However, the electric dipole is strongly affected as the refractive index become more metal like and perturbs the high electric field near the PCM layer. The controllability of the electric dipole allows the PCM to operate as a switchable mode reflector. Therefore, the electric dipole is mainly considered in this study. The effect of geometrical parameters, the PCM thickness and also the type of PCM have been investigated to optimize the reflectance profile. The performance of the structure is characterized by the reflectance contrast (RC), the insertion loss (IL), the extinction ratio (ER) and the figure of merit (FOM).

The aim of this study is to fix the electric dipole resonance at 1550 nm because its important in the telecommunication. However, the design optimization can be carried out for any wavelength as desired. The numerical results show that by increasing the height, the diameter needs to be decreased in order to optimize ED at 1550 nm. When the height is 215 nm and diameter is 646.8 nm led to better performance with IL = 1.02 dB and the ER = 10.5 dB. We also have shown thinner PCM thickness yields better performance of the reflector. Finally, we also have shown that by using GSST instead of GST, the device performance can be further improved.

Acknowledgments. This work was supported by Science Achievement Scholarship of Thailand (SAST), and the software support from City, University of London.

Disclosures. The authors declare no conflicts of interest.

Data availability. Data underlying the results presented in this paper are not publicly available at this time but may be obtained from the authors upon reasonable request.

Optics EXPRESS

References

1. O. Quevedo-Teruel, H. Chen, A. Díaz-Rubio, G. Gok, A. Grbic, G. Minatti, E. Martini, S. Maci, G. V. Eleftheriades, M. Chen, N. I. Zheludev, N. Papasimakis, S. Choudhury, Z. A. Kudyshev, S. Saha, H. Reddy, A. Boltasseva, V. M. Shalaev, A. V. Kildishev, D. Sievenpiper, C. Caloz, A. Al, Q. He, L. Zhou, G. Valerio, E. Rajo-Iglesias, Z. Sipus, F. Mesa, R. Rodríguez-Berral, F. Medina, V. Asadchy, S. Tretyakov, and C. Craeye, "Roadmap on metasurfaces," J. Opt. **21**(7), 073002 (2019).
2. S. Zeng, K. V. Sreekanth, J. Shang, T. Yu, C. K. Chen, F. Yin, D. Baillargeat, P. Coquet, H. P. Ho, A. V. Kabashin, and K. T. Yong, "Graphene-gold metasurface architectures for ultrasensitive plasmonic biosensing," Adv. Mater. **27**(40), 6163–6169 (2015).
3. N. Yu and F. Capasso, "Flat optics with designer metasurfaces," Nat. Mater. **13**(2), 139–150 (2014).
4. N. Meinzer, W. L. Barnes, and I. R. Hooper, "Plasmonic meta-atoms and metasurfaces," Nat. Photonics **8**(12), 889–898 (2014).
5. N. I. Landy, S. Sajuyigbe, J. J. Mock, D. R. Smith, and W. J. Padilla, "Perfect metamaterial absorber," Phys. Rev. Lett. **100**(20), 207402 (2008).
6. J. Y. Rhee, Y. J. Yoo, K. W. Kim, Y. J. Kim, and Y. P. Lee, "Metamaterial-based perfect absorbers," J. Electromagn. Waves Appl. **28**(13), 1541–1580 (2014).
7. T. W. Ebbesen, H. J. Lezec, H. F. Ghaemi, T. Thio, and P. A. Wolff, "Extraordinary optical transmission through sub-wavelenght hole arrays," Nature **391**(6668), 667–669 (1998).
8. R. Mishra, R. Panwar, and D. Singh, "Equivalent circuit model for the design of frequency-selective, terahertz-band, graphene-based metamaterial absorbers," IEEE Magn. Lett. **9**, 1–5 (2018).
9. H. Mohammadi Nemat-Abad, E. Zareian-Jahromi, and R. Basiri, "Design and equivalent circuit model extraction of a third-order band-pass frequency selective surface filter for terahertz applications," Eng. Sci. Technol. Int. J. **22**(3), 862–868 (2019).
10. H. M. Mousa and M. M. Shabat, "Simulation of a symmetry metamaterial waveguide absorber(TE&TM)," Energy Procedia **74**, 597–607 (2015).
11. P. Yu, L. V. Besteiro, Y. Huang, J. Wu, L. Fu, H. H. Tan, C. Jagadish, G. P. Wiederrecht, A. O. Govorov, and Z. Wang, "Broadband metamaterial absorbers," Adv. Opt. Mater. **7**(3), 1800995 (2019).
12. J. B. Pendry, "Negative refraction makes a perfect lens," Phys. Rev. Lett. **85**(18), 3966–3969 (2000).
13. W. He, X. Huang, F. Yang, J. Ran, S. Xie, and B. Gao, "A wide-angle and polarization-insensitive perfect terahertz wave absorber," *The 9th International Symposium on Ultrafast Phenomena and Terahertz Waves*, WI25 (2018).
14. X. G. Peralta, E. I. Smirnova, A. K. Azad, H.-T. Chen, A. J. Taylor, I. Brener, and J. F. O'Hara, "Metamaterials for THz polarimetric devices," Opt. Express **17**(2), 773 (2009).
15. Z. Zhou, T. Zhou, S. Zhang, Z. Shi, Y. Chen, W. Wan, X. Li, X. Chen, S. N. Gilbert Corder, Z. Fu, L. Chen, Y. Mao, J. Cao, F. G. Omenetto, M. Liu, H. Li, and T. H. Tao, "Multicolor T-ray imaging using multispectral metamaterials," Adv. Sci. **5**(7), 1700982 (2018).
16. A. Rampur, D. M. Spangenberg, B. Sierro, P. Hänzi, M. Klimczak, and A. M. Heidt, "Perspective on the next generation of ultra-low noise fiber supercontinuum sources and their emerging applications in spectroscopy, imaging, and ultrafast photonics," Appl. Phys. Lett. **118**(24), 240504 (2021).
17. K. Fan, J. Y. Suen, X. Liu, and W. J. Padilla, "All-dielectric metasurface absorbers for uncooled terahertz imaging," Optica **4**(6), 601 (2017).
18. S. Zeng, D. Baillargeat, H. P. Ho, and K. T. Yong, "Nanomaterials enhanced surface plasmon resonance for biological and chemical sensing applications," Chem. Soc. Rev. **43**(10), 3426–3452 (2014).
19. Y. Li, J. Lin, H. Guo, W. Sun, S. Xiao, and L. Zhou, "A tunable metasurface with switchable functionalities: from perfect transparency to perfect absorption," Adv. Opt. Mater. **8**(6), 1901548 (2020).
20. G. Ma, X. Fan, P. Sheng, and M. Fink, "Shaping reverberating sound fields with an actively tunable metasurface," Proc. Natl. Acad. Sci. U. S. A. **115**(26), 6638–6643 (2018).
21. Y. Yao, R. Shankar, M. A. Kats, Y. Song, J. Kong, M. Loncar, and F. Capasso, "Electrically tunable metasurface perfect absorbers for ultrathin mid-infrared optical modulators," Nano Lett. **14**(11), 6526–6532 (2014).
22. R. Mao, G. Wang, T. Cai, H. Hou, D. Wang, B. Wu, W. Zhang, and Q. Zhang, "Tunable metasurface with controllable polarizations and reflection/transmission properties," J. Phys. D: Appl. Phys. **53**(15), 155102 (2020).
23. Y. Zhang, C. Fowler, J. Liang, B. Azhar, M. Y. Shalaginov, S. Deckoff-Jones, S. An, J. B. Chou, C. M. Roberts, V. Liberman, M. Kang, C. Ríos, K. A. Richardson, C. Rivero-Baleine, T. Gu, H. Zhang, and J. Hu, "Electrically reconfigurable non-volatile metasurface using low-loss optical phase-change material," Nat. Nanotechnol. **16**(6), 661–666 (2021).
24. A. Mandal, Y. Cui, L. McRae, and B. Gholipour, "Reconfigurable chalcogenide phase change metamaterials: a material, device, and fabrication perspective," JPhys Photonics **3**(2), 022005 (2021).
25. J. Siegel, A. Schropp, J. Solis, C. N. Afonso, and M. Wuttig, "Rewritable phase-change optical recording in Ge2Sb2Te5 films induced by picosecond laser pulses," Appl. Phys. Lett. **84**(13), 2250–2252 (2004).
26. B. Gholipour, J. Zhang, K. F. MacDonald, D. W. Hewak, and N. I. Zheludev, "An all-optical, non-volatile, bidirectional, phase-change meta-switch," Adv. Mater. **25**(22), 3050–3054 (2013).
27. A. M. Mio, S. M. S. Privitera, V. Bragaglia, F. Arciprete, C. Bongiorno, R. Calarco, and E. Rimini, "Chemical and structural arrangement of the trigonal phase in GeSbTe thin films," Nanotechnology **28**(6), 065706 (2017).

Optics EXPRESS

28. W. J. Wang, L. P. Shi, R. Zhao, K. G. Lim, H. K. Lee, T. C. Chong, and Y. H. Wu, "Fast phase transitions induced by picosecond electrical pulses on phase change memory cells," Appl. Phys. Lett. **93**(4), 043121 (2008).
29. G. Bruns, P. Merkelbach, C. Schlockermann, M. Salinga, M. Wuttig, T. D. Happ, J. B. Philipp, and M. Kund, "Nanosecond switching in GeTe phase change memory cells," Appl. Phys. Lett. **95**(4), 043108 (2009).
30. W. H. P. Pernice and H. Bhaskaran, "Photonic non-volatile memories using phase change materials," Appl. Phys. Lett. **101**(17), 171101 (2012).
31. M. Suri, O. Bichler, D. Querlioz, B. Traoré, O. Cueto, L. Perniola, V. Sousa, D. Vuillaume, C. Gamrat, and B. Desalvo, "Physical aspects of low power synapses based on phase change memory devices," J. Appl. Phys. **112**(5), 054904 (2012).
32. D. Kuzum, R. G. D. Jeyasingh, B. Lee, and H. S. P. Wong, "Nanoelectronic programmable synapses based on phase change materials for brain-inspired computing," Nano Lett. **12**(5), 2179–2186 (2012).
33. S. Raoux, F. Xiong, M. Wuttig, and E. Pop, "Phase change materials and phase change memory," MRS Bull. **39**(8), 703–710 (2014).
34. C. D. Wright, C. Ríos, H. Bhaskaran, N. Youngblood, W. H. Pernice, X. Li, and Z. Cheng, "Fast and reliable storage using a 5 bit, nonvolatile photonic memory cell," Optica **6**(1), 1–6 (2019).
35. T. Cao, C. Wei, R. E. Simpson, L. Zhang, and M. J. Cryan, "Rapid phase transition of a phase-change metamaterial perfect absorber," Opt. Mater. Express **3**(8), 1101 (2013).
36. C. Zhou, J. Liu, M. Fan, M. Zhou, Q. Yang, X. Deng, and Y. Zhang, "Active magnetic dipole emission by the $Ge_2Sb_2Te_5$ nanodisk," Opt. Lett. **46**(19), 4952–4955 (2021).
37. S. Zhang, K. Zhou, K. Zhou, Q. Cheng, Q. Cheng, L. Lu, B. Li, J. Song, and Z. Luo, "Tunable narrowband shortwave-infrared absorber made of a nanodisk-based metasurface and a phase-change material $Ge_2Sb_2Te_5$ layer," Appl. Opt. **59**(21), 6309–6314 (2020).
38. A. V. Pogrebnyakov, C. Rivero-Baleine, D. H. Werner, H. J. Shin, J. D. Musgraves, J. P. Turpin, J. A. Bossard, K. A. Richardson, N. Podraza, and T. S. Mayer, "Reconfigurable near-IR metasurface based on $Ge_2Sb_2Te_5$ phase-change material," Opt. Mater. Express **8**(8), 2264–2275 (2018).
39. N. Raeis-Hosseini and J. Rho, "Metasurfaces based on phase-change material as a reconfigurable platform for multifunctional devices," Materials **10**(9), 1046 (2017).
40. Y. Zhang, J. B. Chou, J. Li, H. Li, Q. Du, A. Yadav, S. Zhou, M. Y. Shalaginov, Z. Fang, H. Zhong, C. Roberts, P. Robinson, B. Bohlin, C. Ríos, H. Lin, M. Kang, T. Gu, J. Warner, V. Liberman, K. Richardson, and J. Hu, "Broadband transparent optical phase change materials for high-performance nonvolatile photonics," Nat. Commun. **10**(1), 1–9 (2019).
41. J. Hu, J. Li, Q. Zhang, R. Soref, T. Gu, and Y. Zhang, "Broadband nonvolatile photonic switching based on optical phase change materials: beyond the classical figure-of-merit," Opt. Lett. **43**(1), 94–97 (2018).
42. D. S. Chao, F. T. Chen, Y. Y. Hsu, W. H. Liu, C. M. Lee, C. W. Chen, W. S. Chen, M. J. Kao, and M. J. Tsai, "Multi-level phase change memory using slow-quench operation: GST vs. GSST," *International Symposium on VLSI Technology, Systems, and Applications, Proceedings* 39–40 (2009).
43. H. H. Li, "Refractive index of silicon and germanium and its wavelength and temperature derivatives," J. Phys. Chem. Ref. Data **9**(3), 561–658 (1980).
44. I. H. Malitson, "Interspecimen comparison of the refractive index of fused silica," J. Opt. Soc. Am. **55**(10), 1205 (1965).
45. C. Ruiz De Galarreta, I. Sinev, A. M. Arseny, P. Trofimov, K. Ladutenko, S. Garcia-Cuevas Carrillo, E. Gemo, A. Baldycheva, J. Bertolotti, and C. D. Wright, "Reconfigurable multilevel control of hybrid," Optica **7**(5), 476–484 (2020).
46. A. Yadav, H. Zheng, H. Lin, J. Chou, J. Michon, J. Hu, J. Li, K. Richardson, Q. Du, T. Gu, V. Liberman, Y. Zhang, Y. Huang, Z. Han, and Z. Fang, "Broadband Transparent Optical Phase Change Materials," *Conference on Lasers and Electro-Optics, January*, JTh5C.4 (2017).